Original Article

JCBFM

Journal of Cerebral Blood Flow & Metabolism
2021, Vol. 41(1) 182–193

DOI: 10.1177/0271678X20908356
journals.sagepub.com/home/jcbfm
SAGE

Altered task-induced cerebral blood flow and oxygen metabolism underlies motor impairment in multiple sclerosis

Kathryn L West[1], Dinesh K Sivakolundu[1], Mark D Zuppichini[1], Monroe P Turner[1], Jeffrey S Spence[1], Hanzhang Lu[2], Darin T Okuda[3] and Bart Rypma[1,4]

Abstract

The neural mechanisms underlying motor impairment in multiple sclerosis (MS) remain unknown. Motor cortex dysfunction is implicated in blood-oxygen-level-dependent (BOLD) functional magnetic resonance imaging (fMRI) studies, but the role of neural–vascular coupling underlying BOLD changes remains unknown. We sought to independently measure the physiologic factors (i.e., cerebral blood flow (ΔCBF), cerebral metabolic rate of oxygen ($\Delta CMRO_2$), and flow–metabolism coupling ($\Delta CBF/\Delta CMRO_2$), utilizing dual-echo calibrated fMRI (cfMRI) during a bilateral finger-tapping task. We utilized cfMRI to measure physiologic responses in 17 healthy volunteers and 32 MS patients (MSP) with and without motor impairment during a thumb-button-press task in thumb-related (task-central) and surrounding primary motor cortex (task-surround) regions of interest (ROIs). We observed significant ΔCBF and $\Delta CMRO_2$ increases in all MSP compared to healthy volunteers in the task-central ROI and increased flow–metabolism coupling ($\Delta CBF/\Delta CMRO_2$) in the MSP without motor impairment. In the task-surround ROI, we observed decreases in ΔCBF and $\Delta CMRO_2$ in MSP with motor impairment. Additionally, ΔCBF and $\Delta CMRO_2$ responses in the task-surround ROI were associated with motor function and white matter damage in MSP. These results suggest an important role for task-surround recruitment in the primary motor cortex to maintain motor dexterity and its dependence on intact white matter microstructure and neural–vascular coupling.

Keywords

Cerebrovascular circulation, energy metabolism, functional magnetic resonance imaging, motor skills, multiple sclerosis, neural–vascular coupling

Received 12 July 2019; Revised 29 October 2019; Accepted 4 December 2019

Introduction

Multiple sclerosis (MS) is an immune-mediated, demyelinating disorder of the central nervous system (CNS) prominently featuring motor impairments. Most MS studies of motor function have utilized simple, unilateral motor tasks and comparisons between healthy controls (HC) and MS patients (MSP) without motor impairments. These assessments have provided evidence of MS-related functional reorganization and increased extent of activation reflecting a compensatory mechanism to maintain motor functionality.[1–3] Fewer studies have tested this hypothesis by comparing MSP with and without motor impairment.

While unilateral tasks allow for direct imaging assessments of contra- and ipsilateral responses, most activities in daily life require bilateral and interlimb coordination. Interhemispheric communication between motor cortices via callosal conduction pathways is important in bilateral coordination.[4]

[1]School of Behavioral and Brain Sciences, University of Texas at Dallas, Richardson, TX, USA
[2]Department of Radiology, Johns Hopkins University, Baltimore, MD, USA
[3]Department of Neurology and Neurotherapeutics, University of Texas Southwestern Medical Center, Dallas, TX, USA
[4]Department of Psychiatry, University of Texas Southwestern Medical Center, Dallas, TX, USA

Corresponding author:
Kathryn L West, Center for BrainHealth, School of Behavioral and Brain Sciences, University of Texas at Dallas, 2200 W Mockingbird Ln, Dallas, TX 75235, USA.
Email: kathryn.west@utdallas.edu

Thus far, the influence of MS on interhemispheric communication and motor performance has been investigated via resting-state functional connectivity and diffusion magnetic resonance imaging (MRI). These studies show increased motor-network connectivity in early disease and reduced connectivity with increasing structural damage and worse clinical outcomes.[5–7] The present literature suggests that brain plasticity reduces lateralization via increased connectivity between motor cortices to maintain motor function. However, this capacity for plasticity may decline with disease progression and ultimately become unsustainable. The physiologic underpinnings of these processes remain unknown.

Overall, much has been learned about motor dysfunction in MS from previous functional MRI (fMRI) studies. Specifically, these studies have consistently reported MS-related changes in blood-oxygen-level-dependent (BOLD) signal during motor task performance compared to HC. However, the direction of these changes has been less consistent. Some studies report increases in BOLD[3,8–11] and infer that additional resources are needed in MSP for optimal task performance. In contrast, other studies show decreases or no difference in BOLD[11–14] and infer that tissue damage hinders proper neural functioning. This between-study variance hinders meaningful translation to treatment strategies in MS.[15]

While such conflicting conclusions might reflect experimental and MSP sample differences, they also highlight the complexity of comparing BOLD between MSP and HC because it relies on multiple physiologic processes. Indeed, BOLD is a confluence of measures, namely, cerebral blood flow (ΔCBF), cerebral metabolic rate of oxygen ($\Delta CMRO_2$), and neural–vascular coupling (as measured by flow–metabolism ratio; $\Delta CBF/\Delta CMRO_2$), that depend on the finely tuned neural–vascular coupling system.[16] This system is mediated by delicate white matter microstructure components (i.e., astrocytes, myelin, oligodendrocytes), prone to disruption in MS.[17] Because of these complex HC-MS system differences, MS-related BOLD changes cannot be assumed to result from changes in neural activity alone. Therefore, the aim of this study was to utilize dual-echo calibrated fMRI (cfMRI) to independently measure the multiple physiologic processes (i.e., ΔCBF, $\Delta CMRO_2$) that underlie ΔBOLD. To evaluate physiologic changes specific to the primary motor cortex, we acquired cfMRI data during a bilateral finger-tapping task in HC as well as MSP with and without motor impairments.

Methods

Participants

Thirty-nine MSP and 19 HC were recruited from the University of Texas Southwestern (UTSW) Medical Center MS Clinic, local MS support groups, and from advertisements and flyers distributed throughout the Dallas-Fort-Worth Metroplex. All study procedures were approved by the University of Texas at Dallas and UTSW Medical Center Institutional Review Boards in accordance with the guidelines of the Declaration of Helsinki and Belmont Report.

All participants underwent screening procedures. Individuals enrolled in the study were free from magnetic resonance (MR)-contraindicators, substance abuse, and significant medical, neurological (other than MS), or psychiatric conditions unrelated to their MS disease course. All participants were right-handed, at least high-school educated, and native English speakers. Due to the inclusion of hypercapnia, all individuals were required to be non-smokers with no history of cardiorespiratory or cerebrovascular conditions. All prospective participants underwent the Telephone Interview for Cognitive Status Modified (TICS-m[18]) to ensure cognitive capability (TICS-m score >22), and all eligible participants provided written informed consent.

All MSP had a confirmed relapsing-remitting MS (RRMS) diagnosis by the 2010 McDonald criteria,[19] were >6 months post last exacerbation, were >30 days post corticosteroid treatment, and were either treatment-naive or treatment-stable (>3 months). Concurrent use of CNS-modifying drugs (e.g., antidepressants) was allowed if individuals were treatment-stable.

Clinical assessment

After scanning, all participants underwent neuropsychological evaluations, including four trials of Nine-Hole-Peg Test (NHPT; two dominant hand and two non-dominant hand), fatigue assessment via Modified Fatigue Impact Scale (MFIS[20]), and neurological disability self-report used to calculate Expanded Disability Status Scale (EDSS) scores.[21] The four NHPT trials were averaged to obtain a mean NHPT time for each participant.

Imaging data and acquisition

All imaging was conducted at the UTSW Advanced Imaging Research Center on a Philips 3T MRI system (Philips Medical Systems, Best, the Netherlands) with a 32-channel SENSE RF head coil. High-resolution anatomical data were acquired using a three-dimensional (3D) T_1-weighted magnetization prepared rapid gradient echo (MPRAGE) pulse sequence to provide regions of interest (ROIs) and brain volume with the following parameters: flip angle $= 12^\circ$, 1 mm^3 isotropic voxel-size, matrix size $= 256 \times 204 \times 160$, scan time $\sim$4 min. Dual-echo fMRI incorporating both pseudo-continuous

arterial spin labeling (pCASL; Echo 1, dependent on CBF) and T_2*-weighted BOLD (Echo 2, dependent on both CBF and $CMRO_2$) were acquired using a single-shot echo planar imaging (EPI)-sequence with the following scan parameters: echo time $(TE)_1 = 11$ ms, $TE_2 = 30$ ms, flip angle = 90°, repetition time (TR) = 4000 ms, labeling duration = 1400 ms, post labeling delay = 1450 ms, label offset = 93 mm, in-plane resolution = 3.44 × 3.44 mm, slice thickness = 6 mm, and 150 volumes.[22,23] Diffusion Kurtosis Imaging (DKI) was acquired with a pulsed gradient spin echo sequence with an EPI readout, SENSE factor = 2.2, 1 zero and 2 non-zero b values (1000 s/mm^2 and 2500 s/mm^2) across 30 directions,[24] TR/TE = 6500/69 ms, voxel size = 2.0 × 2.0 mm^2 (reconstructed to 0.88 × 0.88 mm^2), in-plane matrix size = 112 × 112, 65 axial slices, slice thickness = 2.2 mm, no gap, scan time ~15 min. 3D sagittal T_2-weighted fluid-attenuated inversion recovery (T_2-FLAIR) imaging was used to assess RRMS lesion burden with the following scan parameters: effective TR/inversion time (TI)/$TE(TE_{eq})$ = 4800/1600/344(117) ms, turbo spin echo (TSE) readout = 178 echoes, echo-spacing = 3.5 ms, refocusing flip angle = 120°, matrix size = 228 × 227 × 163, and 1.1 mm^3 isotropic resolution (reconstructed to 1 mm^3), SENSE factor = 2.6x2.

Motor task procedures

The motor task was performed using a block design. Participants wore MR-safe headphones and were presented with a 2 Hz auditory rhythm (E-Prime 2.0, Sharpsburg, PA, USA) and a constant central fixation cross. Participants were asked to press and release bilateral thumb buttons every time they heard an auditory stimulus and response time was recorded. Stimuli were presented across 2 runs with 12, 32-s interleaved (6 task and 6 rest) blocks per run. Each run lasted 384 s and the entire motor task lasted ~13 min.

Hypercapnia procedures

Hypercapnia breathing challenge was performed to obtain an estimate of M[25] for each subject using the dual-echo fMRI sequence (see "Imaging data and acquisition" section) as described in previous work.[23,26] Participants were given a two-way non-rebreathing valve/mouthpiece (Hans Rudolph, 2600 series, Shawnee, KS, USA) for controlled air inhalation from a Douglas bag. For the first 4 min, participants received room air (~0.03% CO_2: 21% O_2: 78% N_2), followed by 6 min of hypercapnic gas mixture (5% CO_2: 21% O_2: 74% N_2). A nose clip ensured breathing via mouthpiece. A capnograph device (Capnogard, Model 1265, Novametrix Medical Systems, CT, USA) was used to monitor end-tidal CO_2 and breathing rate and a pulse oximeter (MEDRAD Veris, Pittsburgh, PA, USA) was used to monitor heart rate and arterial oxygen saturation. Participants focused on a central fixation cross throughout the task.

Data analysis

Cortical parcellation was performed using Freesurfer[27] via the high-resolution MPRAGE image in native space for each participant. For each individual, based on the Freesurfer parcellations from the Desikan-Killiany atlas,[28] anatomical ROIs were defined as the primary motor cortex (M1; comprising the precentral gyrus; Brodmann Area 4) and the gray matter (GM) cortex. Brain parenchymal fraction (BPF[29]) was calculated as a metric for brain atrophy.

All cfMRI data were processed via Analysis of Functional Neuroimages package[30] similar to previous work.[23,26] All Echo 2 (BOLD) images were motion corrected by realignment to the first Echo 2 functional image of the first run and subsequently co-registered to the MPRAGE anatomical image. The realignment and coregistration transformation matrices were applied to the Echo 1 (pCASL) images. All images were high-pass filtered (0.0039 Hz), and smoothed (8 mm Gaussian kernel). For Echo 1 (pCASL), labeled images were surround subtracted from control images to obtain CBF-weighted images to match the time resolution of BOLD images.[31] Similarly, BOLD images were surround averaged to minimize the effects from pCASL.[31] Echo 1 (CBF) and Echo 2 (BOLD) time series were input into a general linear model with a task-related block function and the six motion regressors as covariates to generate voxel-wise baseline (β_0-) and task-related (β_1-) values, and T-statistics.

Hypercapnia data were pre-processed similarly. The first 2 min of the hypercapnia portion of the time series were discarded to allow for blood-flow stabilization. Average normocapnia and hypercapnia BOLD and CBF images were used to calculate voxel-wise percentage signal change (PSC) images, reflecting hypercapnia-induced change from room air after correcting for pCASL labeling efficiency during hypercapnia.[22,23] The GM mask was applied to the PSC images, and the average PSC images from the intersecting top 10% of BOLD and CBF voxels were used to calculate M for each participant,[25] with $\alpha = 0.38$[32] and $\beta = 1.33$[33] via equation (1)[25]

$$M = \frac{\frac{\Delta BOLD}{BOLD_0}}{\left(1 - \frac{CBF}{CBF_0}^{\alpha-\beta}\right)} \quad (1)$$

which assumes that neural metabolism ($CMRO_2$) is not significantly affected by hypercapnia conditions. M has been shown to have reduced variability utilizing GM.[34] However, we wanted to investigate potential influences of regional differences in M. Thus, we calculated M similarly using the M1 mask instead of the GM mask. We observed lower M values in both groups but no significant differences between groups and as a result, no effect on any of the subsequent group $CMRO_2$ differences (see Supplemental Table 2).

Then, for each individual, $CMRO_2$ was calculated using M from hypercapnia and changes in BOLD and CBF from the motor task[25] via equation (2) where $\Delta x/x_0$ reflects PSC and x/x_0 reflects proportional change.

$$\frac{CMRO_2}{CMRO_{2|0}} = \left(1 - \frac{\frac{\Delta BOLD}{BOLD_0}}{M}\right)^{1/\beta} \frac{CBF}{CBF_0}^{(1-\alpha/\beta)} \quad (2)$$

Mean ΔBOLD, ΔCBF, and $\Delta CMRO_2$ PSC were calculated for each participant from all voxels in (a) the task-central ROI, comprised of statistically significant voxels ($T > 1.96$) in both BOLD and CBF images and (b) the task-surround ROI comprised of the surrounding voxels in M1 ($T < 1.96$). While most previous studies have evaluated only significant ($T > 1.96$) ROIs, previous work comparing younger and older adults with a variety of thresholds (e.g., $T > 1.96$, top several voxels, whole anatomical ROI) have shown that the nature of the age differences sometimes depends on how the ROI is chosen.[35–38] Additionally, in MS literature, increased spatial extent of activation has been proposed as a potential mechanism mediating performance. On the basis of results like these, we utilized the task-central and task-surround approach to investigate differing patterns of activation. In addition to block-wise averages from the general linear model, we calculated average task (32 s) and rest (32 s) time series across all task and rest blocks (12 each) voxel-wise and subsequently averaged across voxels within each ROI (task-central and task-surround) for ΔBOLD, ΔCBF, and $\Delta CMRO_2$ for each participant. The time point prior to the start of task was taken as the baseline value to minimize return-to-baseline influences.

In our model, neural–vascular coupling is indexed by the ratio of changes in CBF to changes in $CMRO_2$ ($\Delta CBF/\Delta CMRO_2$). ΔCBF is the output from pCASL which directly measures arterial blood flow. On the other hand, $\Delta CMRO_2$ is calculated more indirectly (see equation (2)) as a function of changes in CBF and BOLD during both task and hypercapnia experiments. Thus, while $\Delta CBF/\Delta CMRO_2$ reflects the communication between the neural and vascular systems, it is inherently indirect to the extent that we cannot directly measure neural activity as in electrophysiological measures (e.g., electroencephalography).

T_2-FLAIR images were used to calculate total lesion volume (TLV) via the lesion-prediction algorithm in the Lesion Segmentation Toolbox (LST v2.0.15). DKI images were corrected for eddy-current distortions and motion using FMRIB Software Library[39] (FSL v5.0.9; Oxford, UK) EDDY tool and co-registered to MPRAGE. Kurtosis analysis was conducted using the Diffusion Kurtosis Estimator[40] software to obtain estimates of fractional anisotropy (FA) and radial kurtosis (RK). FA images were aligned to whole-brain skeletons using Tract-Based Spatial Statistics[41] ($FA > 0.4$) yielding white-matter-skeleton RK estimates for each participant. The JHU ICBM-DTI-81 white-matter atlas was applied to each skeletonized RK map to obtain average RK from the corpus callosum (CC) for each participant.[42]

Statistical analysis

Statistical analyses were conducted using SPSS (2017, Version 25.0; IBM Corp., Armonk, NY, USA). Equality of variance was tested via Levene's test, and group comparisons were conducted via independent samples t test ($p < 0.05$). All α thresholds were corrected for multiple comparisons via false discovery rate.[43] Associations were assessed using Spearman correlation ($p < 0.05$). BOLD and CBF PSC outliers were removed via median absolute deviation[44] ($k = 1.4826$, $b = 3$) by group, resulting in a final cohort of 32 MSP and 17 HC described in Table 1.

Results

Table 1 describes the HC and MSP sample characteristics. There were no significant differences between the two groups in age, sex, education, BPF, or button-press frequency in the scanner. There were significant increases in NHPT time ($p = 0.001$) and MFIS score ($p < 0.001$) in MSP.

We evaluated M and PSC differences in physiologic parameters in the two ROIs (task-central and task-surround). M was similar to previous results in healthy adults.[23,45,46] There is minimal work in MS using cfMRI to compare with, but we observed no significant MS-HC differences in M ($p = 0.355$). Figure 1(a) to (c) shows average task-related ΔBOLD, ΔCBF, and $\Delta CMRO_2$ PSC for HC and MSP. In the task-central ROI, there were no significant differences in ΔBOLD, but MSP had significantly higher ΔCBF ($p = 0.001$) and $\Delta CMRO_2$ ($p = 0.003$) compared with HC (see Table 2). There were no differences in the task-surround ROI (see Table 2). To further evaluate differences within

Table 1. Sample characteristics.

	HC ($n = 17$)	MSP ($n = 32$)	p
Demographics			
Age (years)	43.18 (11.01)	46.69 (10.71)	0.285
Sex (% female)	76.47	56.25	0.162[a]
Education (years)	17.50 (1.71)	16.06 (2.61)	0.053
Brain parenchymal fraction (%)	73.69 (3.69)	70.61 (6.27)	0.078
Patient characteristics			
Disease duration (years)	–	10.68 (7.93)	–
Lesion volume (mL)	–	7.55 (9.84)	–
EDSS	–	3.27 (1.88)	–
Modified Fatigue Impact Scale	15.56 (12.85)	39.77 (15.15)	<0.001
Task performance			
Button-press frequency (Hz)	1.94 (0.05)	1.92 (0.07)	0.422
Nine-Hole-Peg Test (s)	19.17 (2.66)	24.73 (7.99)	0.001

Note: Values are represented as mean (standard deviation). EDSS: Expanded Disability Status Scale; MSP: multiple sclerosis patients; HC: healthy controls.
[a]Pearson χ^2 test.

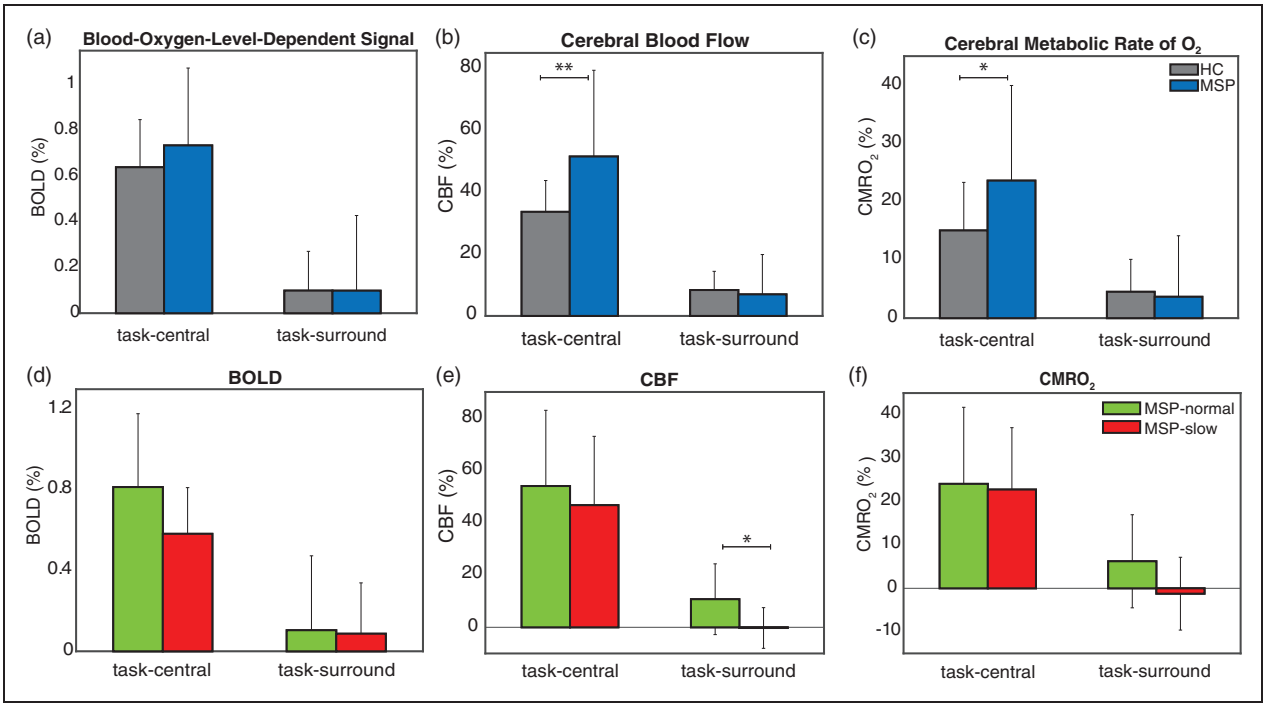

Figure 1. (a to c) Mean (std) of BOLD, CBF, and $CMRO_2$, from HC and MSP in the task-central and task-surround ROIs. (d to f) Mean (std) of MSP-normal and MSP-slow BOLD, CBF, and $CMRO_2$ in the task-central and task-surround ROIs. *$p < 0.05$, **$p < 0.01$. BOLD: blood-oxygen-level-dependent; CBF: cerebral blood flow; $CMRO_2$: cerebral metallic rate of O_2; MSP: multiple sclerosis patients; HC: healthy controls.

the MSP group with respect to motor disability, we split MSP by their NHPT time (cutoff = $NHPT_{HC,mean} + 1.5 \times NHPT_{HC,std} = 23.17$ s) as MSP-normal (< 23.17 s; n = 19, NHPT = 20.28 ± 1.81 s) and MSP-slow (> 23.17 s; n = 9, NHPT = 33.22 ± 8.39 s); 1.5 standard deviations above the HC_{mean} reflect the 6.68% lowest performing individuals in the normal population. MSP-normal and MSP-slow groups did not differ by age, gender, education, M1 size, button-press frequency, or MFIS score, but MSP-slow had significantly lower BPF ($p = 0.006$), longer disease duration ($p = 0.029$), higher T_2-lesion volume ($p = 0.009$), and increased EDSS ($p = 0.005$; see Supplementary Table 1).

Table 2. Mean (standard deviation) values from (top) HC and MSP in the task-central and task-surround ROIs and (bottom) MSP-normal and MSP-slow.

	HC	MSP	Levene's *p*	*T*-test *p*
M	0.107 (0.07)	0.088 (0.05)	0.045	0.355
Task-central ROI				
ΔBOLD (%)	0.639 (0.21)	0.735 (0.34)	0.104	0.295
ΔCBF (%)	33.63 (10.13)	51.51 (27.87)	0.003	0.002
$\Delta CMRO_2$ (%)	15.06 (8.26)	23.62 (16.34)	0.022	0.019
No. of voxels	5597.00 (3253.59)	5014.84 (3942.79)	0.578	0.605
Task-surround ROI				
ΔBOLD (%)	0.099 (0.17)	0.099 (0.33)	0.175	0.997
ΔCBF (%)	8.37 (6.04)	6.96 (12.88)	0.027	0.605
$\Delta CMRO_2$ (%)	4.52 (5.57)	3.66 (10.48)	0.101	0.756
No. of voxels	45,835.35 (3967.29)	46,239.13 (6137.46)	0.074	0.808
	MSP-normal	MSP-slow		
Task-central ROI				
ΔBOLD (%)	0.815 (0.363)	0.583 (0.229)	0.207	0.065
ΔCBF (%)	54.03 (28.95)	46.71 (26.32)	0.700	0.490
$\Delta CMRO_2$ (%)	24.07 (17.65)	22.76 (14.26)	0.212	0.834
Task-surround ROI				
ΔBOLD (%)	0.105 (0.369)	0.087 (0.252)	0.505	0.890
ΔCBF (%)	10.74 (13.53)	−0.26 (7.78)	0.136	0.019
$\Delta CMRO_2$ (%)	6.23 (10.73)	−1.24 (8.39)	0.324	0.054

Note: Levene's test and t tests were performed with p values displayed. MSP: multiple sclerosis patients; HC: healthy controls; ROI: region of interest; BOLD: blood-oxygen-level-dependent; CBF: cerebral blood flow; $CMRO_2$: cerebral metallic rate of O_2.

Figure 1(d) to (f) shows average ΔBOLD, ΔCBF, and $\Delta CMRO_2$ in the task-central and task-surround ROIs in MSP-normal and MSP-slow. There were no differences between MSP-normal and MSP-slow groups in the task-central ROI, suggesting that, in this ROI, the group-level MSP data (Figure 1(a) to (c)) faithfully reflect the responses from all MSP. In the task-surround ROI, MSP-normal and MSP-slow demonstrate differences in ΔCBF ($p = 0.019$) and in $\Delta CMRO_2$ ($p = 0.054$; see Table 1). This pattern of results illustrates that the group-level MSP data (Figure 1(a) to (c)) represent the average of opposing ΔCBF and $\Delta CMRO_2$ responses from MSP-normal and MSP-slow groups in the task-surround ROI. While, MSP-normal showed similar ΔCBF and $\Delta CMRO_2$ responses compared with HC, MSP-slow had reduced responses. To evaluate the potential effects of significant negative ROIs, we also evaluated the task-negative ROI ($T < -1.96$). The task-negative ROI was ~1% of M1 across all groups, and we did not observe any differences in physiologic parameters between groups (see Supplemental Table 3). Altogether, these results suggest that MSP-slow do not recruit the task-surround ROI which appears to be critical for successful performance of a more complex motor task (i.e., NHPT) that requires increased dexterity.

Next, we evaluated the spatial ROI differences between HC, MSP-normal, and MSP-slow groups. We transformed each participant's anatomical MPRAGE image to Talaraich coordinates and applied this transform to the task-central and task-surround ROIs. ROIs were averaged across each group and threshold to comprise voxels that were included in >25% of participants per group. The group-averaged ROIs are displayed in Figure 2 for task-central (green), task-surround (red), and the positive voxels within task-surround (blue) for each group. The number of voxels per ROI and dice similarity coefficient (DSC[47]) are displayed in Table 3. HC and MSP-normal had 43.0% overlapping task-central ROIs and ~41% of the task-surround ROI was comprised of positive voxels. However, whereas MSP-slow displayed similar task-central ROI spatial overlap with HC and MSP-normal (DSC = 40.6 and 44.0%, respectively), MSP-slow displayed many fewer positive voxels within the task-surround ROI (26.5%). It is important to note that there were no significant group-differences in the number of voxels comprising the task-central ROIs (see Table 2). This demonstrates that MSP have similar extents of the task-central ROI but more varied ROI locations and thus, fewer within-group overlapping voxels compared to HC.

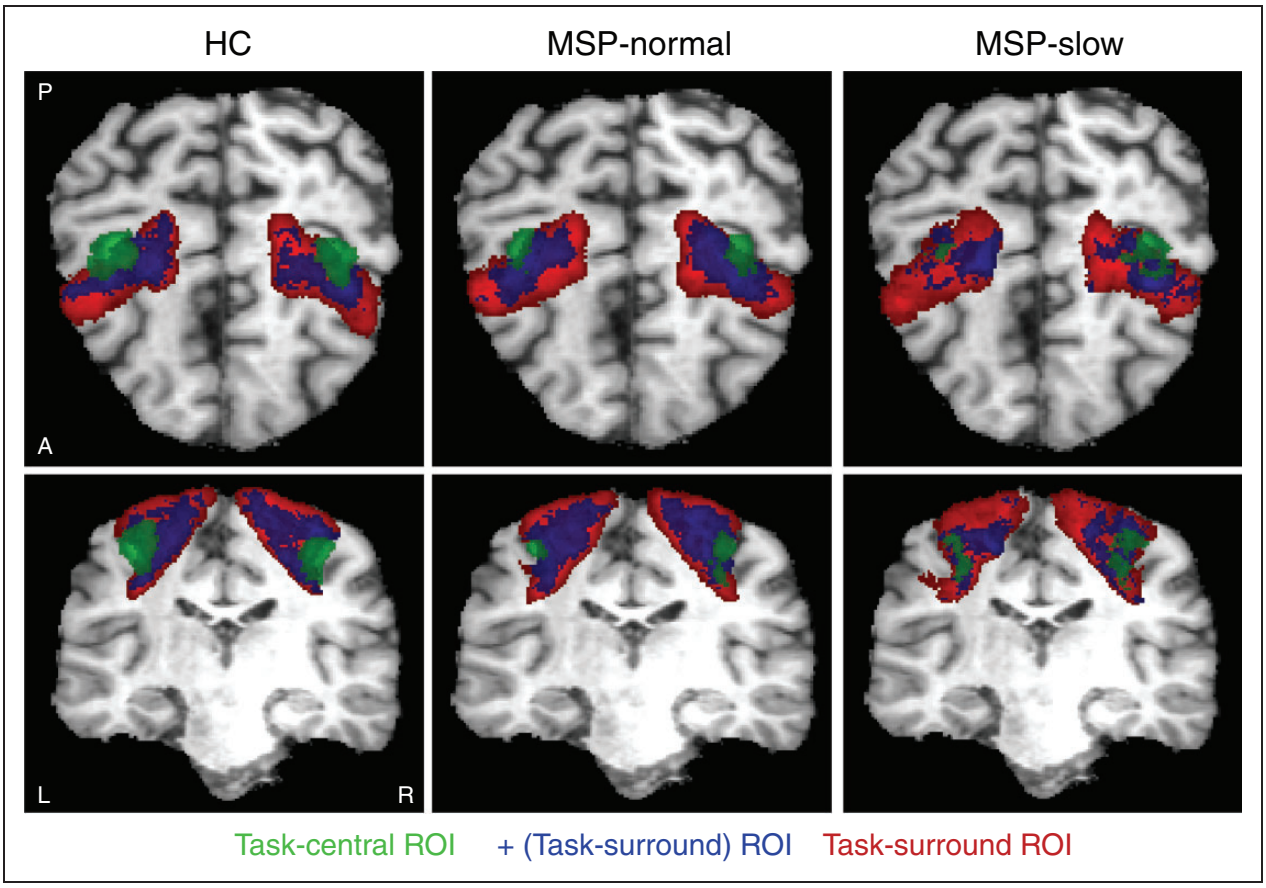

Figure 2. Group-averaged ROIs for (green) task-central, (red) task-surround, and (blue) the positive voxels within task-surround ROI. Talaraich coordinates: $y = -21.00$, $z = 49.00$. MSP: multiple sclerosis patients; HC: healthy controls; ROI: region of interest.

Table 3. Number of voxels in group-averaged ROI (see Figure 2) and DSCs representing spatial overlap of ROIs between groups.

	Task-central ROI	+(Task-surround) ROI	Task-surround ROI
HC	6017	33,636	78,963
MSP-normal	2499	31,907	78,674
MSP-slow	3373	21,065	79,444
DSC (HC:MSP-normal)	0.430	0.643	0.904
DSC (HC:MSP-slow)	0.406	0.502	0.868
DSC (MSP-normal:MSP-slow)	0.440	0.500	0.885

DSC: dice similarity coefficient; MSP: multiple sclerosis patients; HC: healthy controls; ROI: region of interest.

We then evaluated changes in ΔCBF and $\Delta CMRO_2$ through the duration of the task block. Figure 3(a) and (c) shows the average ΔCBF and $\Delta CMRO_2$ time series during rest- and task-blocks, and Figure 3(b) and (d) displays the average task-related flow–metabolism coupling ratio ($\Delta CBF/\Delta CMRO_2$) for each group in the task-central and task-surround ROIs. In the task-central ROI, results were similar to those in Figure 1, both MSP-normal and MSP-slow had increased ΔCBF and $\Delta CMRO_2$ compared to HC (Figure 3(a)). However, MSP-normal had significantly higher flow–metabolism coupling ratio compared to HC and MSP-slow (Figure 3(b)). Again, similar to Figure 1, in the task-surround ROI (Figure 3(c)), MSP-slow had decreased ΔCBF and $\Delta CMRO_2$; however, Figure 3(c) illustrates the unique decline in ΔCBF to baseline levels

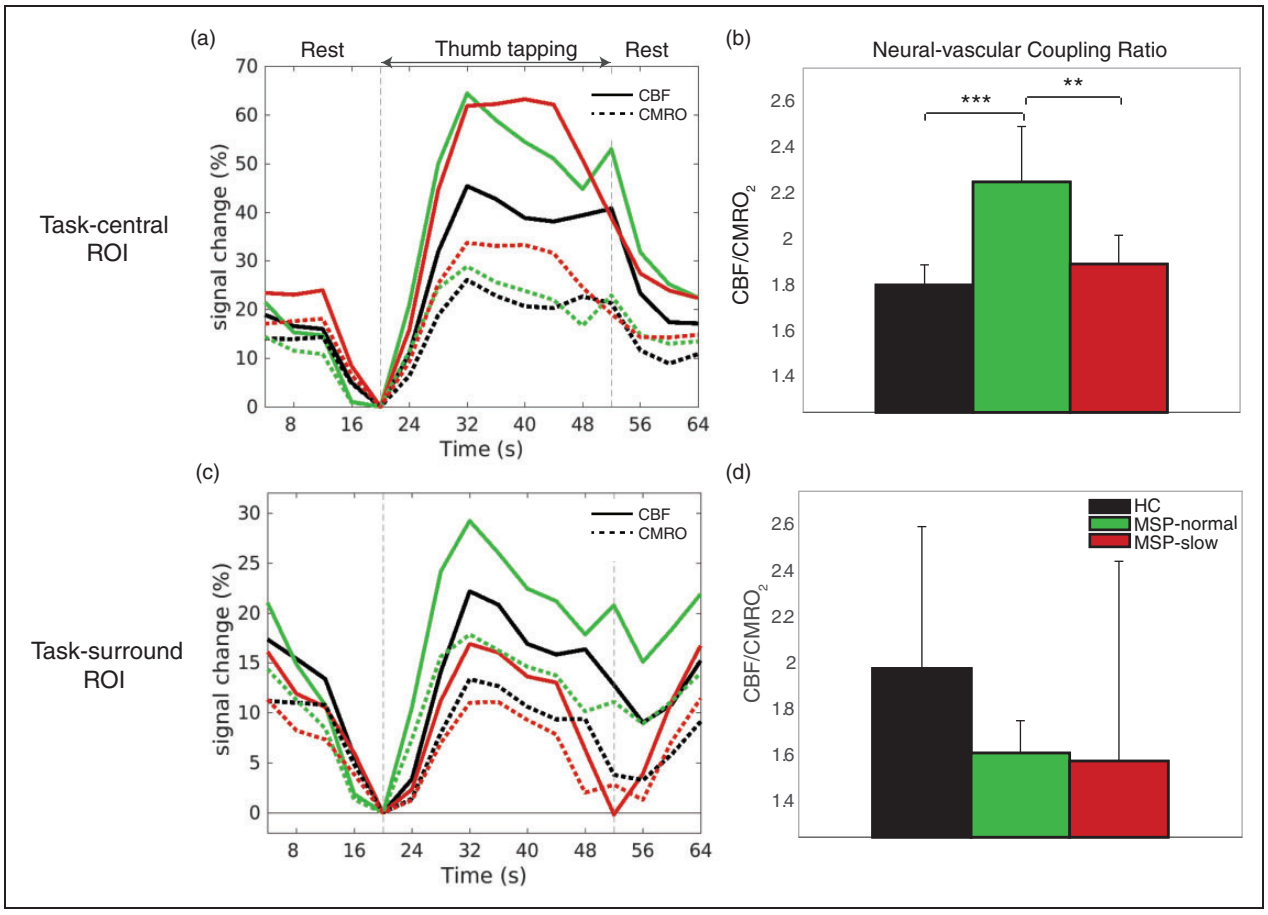

Figure 3. (a and c) Average (solid) CBF and (dashed) $CMRO_2$ percentage signal change time series in task-central and task-surround ROIs during rest and thumb-tapping motor task blocks for (black) HC, (green) MSP-normal, and (red) MSP-slow groups. For each time series, the final rest time point (i.e., 20 s) was used as the baseline value. (b and d) Neural–vascular coupling ratio ($CBF/CMRO_2$) in task-central and task-surround ROIs during thumb-tapping motor task blocks for (black) HC, (green) MSP-normal, and (red) MSP-slow groups (mean $\pm$ std). CBF: cerebral blood flow; $CMRO_2$: cerebral metallic rate of O_2; MSP: multiple sclerosis patients; HC: healthy controls; ROI: region of interest. $^*p < 0.05$, $^{**}p < 0.01$, $^{***}p < 0.001$.

in MSP-slow at the end of the task block. Overall, MSP display lower flow–metabolism coupling in the task-surround ROI compared to HC (Figure 3(d)).

Finally, we assessed the association of ΔCBF and $\Delta CMRO_2$ from the task-surround ROI with NHPT performance and white matter damage in the CC. Figure 4(a) and (b) illustrates significant negative correlations between ΔCBF and $\Delta CMRO_2$ and NHPT time in MSP but not in HC. Figure 4(c) and (d) shows significant positive correlations between ΔCBF and $\Delta CMRO_2$ and RK in the CC in MSP but not in HC. All correlations remained significant after controlling for age and gender. Thus, decreased ΔCBF and $\Delta CMRO_2$ in the task-surround ROI was associated with worse motor performance (longer NHPT time) and more CC white matter damage (lower RK). There were no significant correlations in MSP between BPF, disease duration, TLV, EDSS, and ΔCBF or $\Delta CMRO_2$ in the task-surround ROI or between NHPT time or RK and ΔCBF or $\Delta CMRO_2$ from task-central ROI. Thus, while there are significant differences in clinical metrics (e.g., TLV) between MSP-normal and MSP-slow, changes in CBF and $CMRO_2$ are only related to NHPT performance and RK.

Discussion

In the present study, we sought to undertake examination of the physiologic underpinnings of motor slowing in MS. The MSP were stratified into those with and without clinically relevant motor disability. We utilized dual-echo calibrated imaging while participants performed a bilateral button-press task that invoked neural–vascular activity in M1. The use of dual-echo imaging permitted separation of the constituent neural and vascular components mediating these clinically relevant changes. In M1, we observed increased ΔCBF and $\Delta CMRO_2$ responses in all MSP compared to HC

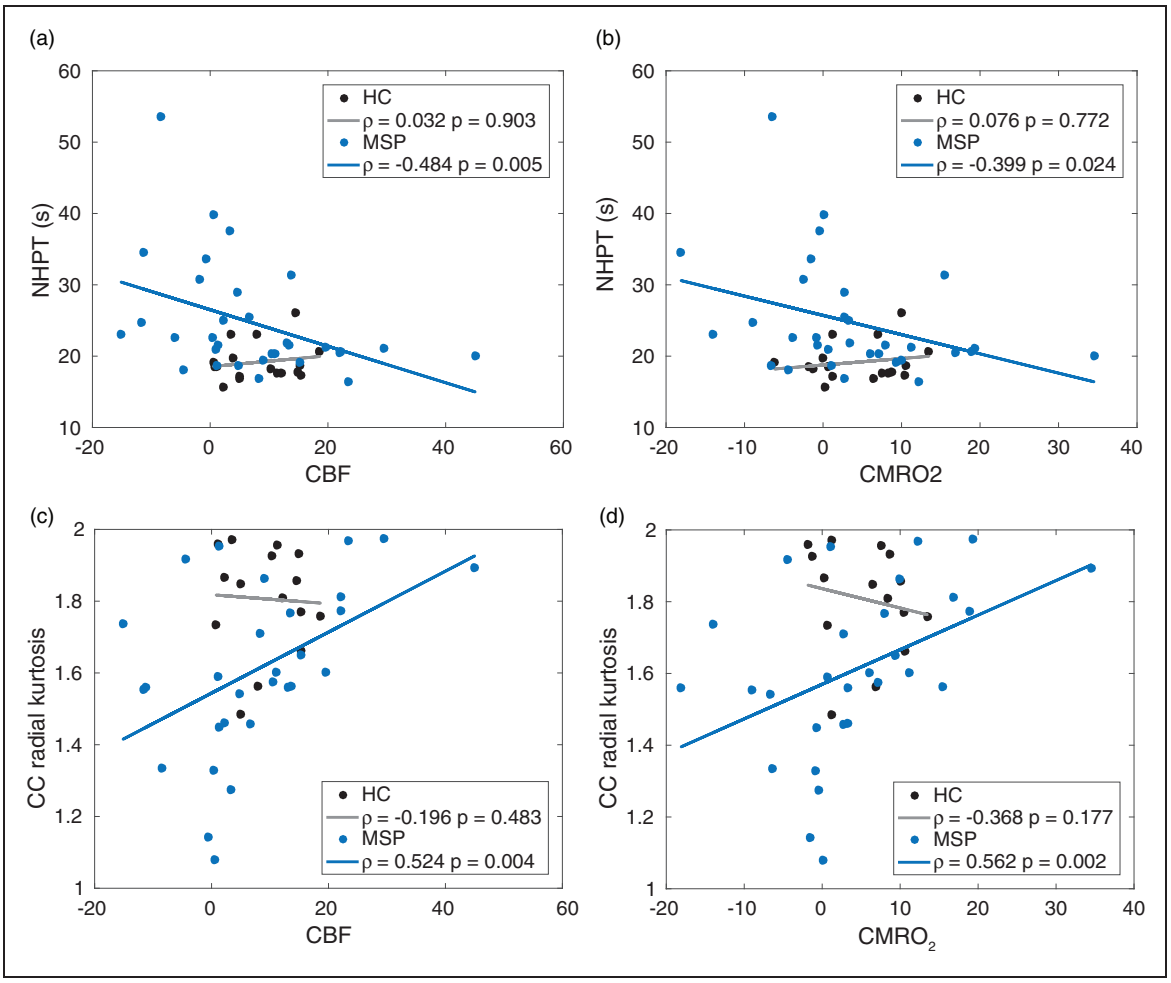

Figure 4. Correlations between NHPT time and (a) CBF and (b) $CMRO_2$ from the task-surround ROI in (black) HC and (blue) MSP (top). Correlations between CC radial kurtosis and (c) CBF and (d) $CMRO_2$ from the task-surround ROI in (black) HC and (blue) MSP (bottom). All Pearson correlation coefficients (ρ) are displayed and were evaluated as significant ($p < 0.05$) in MSP but not HC. NHPT: Nine-Hole-Peg Test; CBF: cerebral blood flow; $CMRO_2$: cerebral metallic rate of O_2; MSP: multiple sclerosis patients; HC: healthy controls; CC: corpus callosum.

in the task-central ROI. In the task-surround ROI, MSP-slow showed reduced ΔCBF and $\Delta CMRO_2$ compared to MSP-normal. Anatomically, MSP-slow had a less coherent task-central ROI between individuals and had fewer positively responding voxels in the task-surround ROI. These results appear to be driven by disruption of an organized flow–metabolism (i.e., neural–vascular) response. Inspection of the time-series data showed that ΔCBF response collapsed in MSP-slow during the task block. Finally, ΔCBF and $\Delta CMRO_2$ responses in the task-surround ROI correlate strongly with motor performance and white matter damage in MSP. These results suggest that spatially expanding activity is critical to maintaining task performance, especially as task demand increases. Such expansion appears to depend on the integrity of neural–vascular coupling.

Most previous work has utilized BOLD fMRI to study motor function in MS. BOLD provides insight regarding physiologic changes but reflects an amalgam of physiologic processes. This property of BOLD is exemplified in the current study by similar ΔBOLD responses between groups and regions (see Figure 1) but drastic differences in ΔCBF and $\Delta CMRO_2$. Thus, the use of cfMRI permits assessment of these underlying changes in blood flow and neural activity in MSP, which are not evident using BOLD alone, and provides an explanation for inconsistencies in literature. Additionally, these results have implications for conclusions of MS-related changes in neural activity based on changes in BOLD alone.[23,25,26]

While all MSP displayed equivalent increases in ΔCBF and $\Delta CMRO_2$ in the task-central ROI compared to HC (see Figure 1), the MSP groups differed

greatly in the task-surround ROI, wherin MSP-slow had reduced ΔCBF and $\Delta CMRO_2$. As all participants performed similarly on the button-press task, these results suggest that recruitment capability beyond the locus of the thumb is vital for more complex and increased-dexterity tasks, such as the NHPT. The present technique of task-central and task-surround ROIs permitted investigation of the patterns of activation within both the supra-threshold voxels and the anatomical ROI. Similar methods have revealed important between-population differences in other literature.[35–37] Additionally, previous studies have shown that non-disabled MSP display increased activation extent with increasing task demand.[1] This proposed mechanism is supported in our study by increased $\Delta CBF/\Delta CMRO_2$ in task-central ROI in MSP-normal (see Figure 3) and the strong positive correlations between ΔCBF and $\Delta CMRO_2$ from the task-surround ROI and NHPT performance (see Figure 4). Thus, our results suggest that recruitment capability is maintained in MSP-normal but hindered in MSP-slow during more complex tasks. Figure 4 also exhibits a negative correlation between ΔCBF and $\Delta CMRO_2$ and CC RK. Thus, increased callosal demyelination or axonal loss in MSP-slow might hinder transcallosal communication[48] and the integrity of the neural–vascular coupling unit (see Figure 4); more work is certainly needed to explore this relationship using advanced imaging techniques.

In the present study, we did not observe differences in the spatial extent of the task-central ROI between groups, suggesting that thumb motion remains localized to the primary motor cortex. However, Figure 2 and Table 3 demonstrate the inconsistency of the task-central ROI localization between MSP compared to HC. Other studies have shown functional reorganization via cortical recruitment in MSP.[2,14,49] The disparity in a coherent locus of activation in MSP-slow could reflect cortical damage leading to reorganization. However, these individuals also have significant white matter damage, possibly limiting cortical adaptive capacity, resulting in irreversible clinical deficits.[8] We limited the current study to focus on M1. It would be of interest to investigate ΔCBF and $\Delta CMRO_2$ alterations and/or adaptations in supplementary motor and premotor cortex.

The present study utilized a simple bilateral thumb-button-press task during MRI scanning. This task provided robust bilateral M1 activity and was well-tolerated by all participants; however, more could be learned in future studies using alternating unilateral or more complex bilateral motor tasks. For example, it is apparent in Figure 2 that the group-level task-central ROI in MSP-slow is more localized to the right hemisphere. One plausible explanation for this result is that, because all participants were right-handed, MSP-slow required increased effort focused on the non-dominant hand compared to HC and MSP-normal to coordinate a bimanual response.[50] Thus, differences in physiologic parameters between unilateral and bilateral tasks would provide further insight into the role of white matter microstructure in interhemispheric interactions, the roles of excitatory and inhibitory signaling, their relationships to motor performance,[51] and how they are affected in MS. Considering previous work demonstrating progressive changes in functional connectivity in motor networks related to performance and fatigue in MS,[5,7,52,53] future studies combining functional connectivity, diffusion MRI, and cfMRI metrics will provide important insights into the underpinnings of the clinical motor deficits observed in MS.

The present study independently measured ΔBOLD, ΔCBF, and $\Delta CMRO_2$ in M1 during a bilateral motor task to evaluate the physiologic underpinnings of clinical motor impairment in MS. In MSP-slow, we observed decreases in ΔCBF and $\Delta CMRO_2$ in the task-surround region of M1 but not in the task-central region. While more work is certainly needed, significant associations between ΔCBF, $\Delta CMRO_2$, motor performance, and white matter damage in MSP suggest an important role for spatially expanding M1 activity to maintain motor dexterity and its dependence on intact neural–vascular coupling.

Funding

The author(s) disclosed receipt of the following financial support for the research, authorship, and/or publication of this article: This work was supported by National Multiple Sclerosis Society (RG150704951 to BR), National Institutes of Health (1R01AG047972 to BR), and the Friends of BrainHealth Visionary Distinguished New Scientist Award (to KLW).

Declaration of conflicting interests

The author(s) declared the following potential conflicts of interest with respect to the research, authorship, and/or publication of this article: DTO received advisory and consulting fees from Celgene, EMD Serono, Genentech, Genzyme, and Novartis and research support from Biogen. The remaining authors declared no potential conflicts of interest with respect to the research, authorship, or publication of this article.

Authors' contributions

KLW, HL, DTO, and BR conceived and designed the study. KLW, DKS, MDZ, and MPT conducted the experiments. KLW, DKS, MDZ, MPT, and JSS performed data analysis. KLW wrote the manuscript and all authors revised the manuscript.

Data accessibility statement

The data sets generated and analyzed during this study are available from the corresponding author upon request.

ORCID iD

Kathryn L West https://orcid.org/0000-0003-3059-8923

Supplemental material

Supplemental material for this article is available online.

References

1. Rocca MA, Gatti R, Agosta F, et al. Influence of task complexity during coordinated hand and foot movements in MS patients with and without fatigue: a kinematic and functional MRI study. *J Neurol* 2009; 256: 470–482.
2. Pantano P, Mainero C and Caramia F. Functional brain reorganization in multiple sclerosis: evidence from fMRI studies. *J Neuroimaging* 2006; 16: 104–114.
3. Rocca MA, Falini A, Colombo B, et al. Adaptive functional changes in the cerebral cortex of patients with non-disabling multiple sclerosis correlate with the extent of brain structural damage. *Ann Neurol* 2002; 51: 330–339.
4. Gerloff C and Andres FG. Bimanual coordination and interhemispheric interaction. *Acta Psychol (Amst)* 2002; 110: 161–186.
5. Rocca MA, Valsasina P, Leavitt VM, et al. Functional network connectivity abnormalities in multiple sclerosis: correlations with disability and cognitive impairment. *Mult Scler J* 2018; 24: 459–471.
6. Kern KC, Sarcona J, Montag M, et al. Corpus callosal diffusivity predicts motor impairment in relapsing-remitting multiple sclerosis: a TBSS and tractography study. *Neuroimage* 2011; 55: 1169–1177.
7. Faivre A, Rico A, Zaaraoui W, et al. Assessing brain connectivity at rest is clinically relevant in early multiple sclerosis. *Mult Scler J* 2012; 18: 1251–1258.
8. Reddy H, Narayanan S, Arnoutelis R, et al. Evidence for adaptive functional changes in the cerebral cortex with axonal injury from multiple sclerosis. *Brain* 2000; 123: 2314–2320.
9. Wegner C, Filippi M, Korteweg T, et al. Relating functional changes during hand movement to clinical parameters in patients with multiple sclerosis in a multi-centre fMRI study. *Eur J Neurol* 2008; 15: 113–122.
10. White AT, Lee JN, Light AR, et al. Brain activation in multiple sclerosis: a BOLD fMRI study of the effects of fatiguing hand exercise. *Mult Scler* 2009; 15: 580–586.
11. Sweet LH, Rao SM, Primeau M, et al. Functional magnetic resonance imaging response to increased verbal working memory demands among patients with multiple sclerosis. *Hum Brain Mapp* 2006; 27: 28–36.
12. Genova HM, Hillary FG, Wylie G, et al. Examination of processing speed deficits in multiple sclerosis using functional magnetic resonance imaging. *J Int Neuropsychol Soc* 2009; 15: 383–393.
13. Hubbard NA, Turner M, Hutchison JL, et al. Multiple sclerosis-related white matter microstructural change alters the BOLD hemodynamic response. *J Cereb Blood Flow Metab* 2016; 36: 1872–1884.
14. Lee M, Reddy H, Johansen-Berg H, et al. The motor cortex shows adaptive functional changes to brain injury from multiple sclerosis. *Ann Neurol* 2000; 47: 606–613.
15. Iannetti GD and Wise RG. BOLD functional MRI in disease and pharmacological studies: room for improvement? *Magn Reson Imaging* 2007; 25: 978–988.
16. Iadecola C. The neurovascular unit coming of age: a journey through neurovascular coupling in health and disease. *Neuron* 2017; 96: 17–42.
17. Wegner C, Filippi M, Korteweg T, et al. Exploring neural efficiency in multiple sclerosis patients during the symbol digit modalities test: a functional magnetic resonance imaging Study. *Neuroimage* 2017; 7: 474–482.
18. Brandt J, Spencer M and Folstein M. The telephone interview for cognitive status. *Neuropsychiatry Neuropsychol Behav Neurol* 1988; 1: 111–118.
19. Polman CH, Reingold SC, Banwell B, et al. Diagnostic criteria for multiple sclerosis: 2010 revisions to the Mcdonald criteria. *Ann Neurol* 2011; 69: 292–302.
20. Flachenecker P, Kümpfel T, Kallmann B, et al. Fatigue in multiple sclerosis: a comparison of different rating scales and correlation to clinical parameters. *Mult Scler J* 2002; 8: 523–526.
21. Verdier-Taillefer MH, Roullet E, Cesaro P, et al. Validation of self-reported neurological disability in multiple sclerosis. *Int J Epidemiol* 1994; 23: 148–154.
22. Aslan S, Xu F, Wang PL, et al. Estimation of labeling efficiency in pseudocontinuous arterial spin labeling. *Magn Reson Med* 2010; 63: 765–771.
23. Hutchison JL, Lu H and Rypma B. Neural mechanisms of age-related slowing: the ΔCBF/ΔCMRO2 ratio mediates age-differences in BOLD signal and human performance. *Cereb Cortex* 2013; 23: 2337–2346.
24. Jones DK, Horsfield MA and Simmons A. Optimal strategies for measuring diffusion in anisotropic systems by magnetic resonance imaging. *Magn Reson Med* 1999; 42: 515–525.
25. Hoge R, Atkinson J, Gill B, et al. Investigation of BOLD signal dependence on cerebral blood flow and oxygen consumption: the deoxyhemoglobin dilution model. *Magn Reson Med* 1999; 42: 849–863.
26. Hubbard NA, Turner MP, Ouyang M, et al. Calibrated imaging reveals altered grey matter metabolism related to white matter microstructure and symptom severity in multiple sclerosis. *Hum Brain Mapp* 2017; 38: 5375–5390.
27. Fischl B, Van Der Kouwe A, Destrieux C, et al. Automatically parcellating the human cerebral cortex. *Cereb Cortex* 2004; 14: 11–22.
28. Desikan RS, Ségonne F, Fischl B, et al. An automated labeling system for subdividing the human cerebral cortex on MRI scans into gyral based regions of interest. *Neuroimage* 2006; 31: 968–980.
29. Rudick RA, Fisher E, Lee J-C, et al. Use of the brain parenchymal fraction to measure whole brain atrophy in relapsing-remitting MS. *Neurology* 1999; 53: 1698–1698.

30. Cox RW. AFNI: software for analysis and visualization of functional magnetic resonance neuroimages. *Comput Biomed Res* 1996; 29: 162–173.
31. Liu TT and Wong EC. A signal processing model for arterial spin labeling functional MRI. *Neuroimage* 2005; 24: 207–215.
32. Grubb RL, Raichle ME, Eichling JO, et al. The effects of changes in $PaCO_2$ on cerebral blood volume, blood flow, and vascular mean transit time. *Stroke* 1974; 5: 630–639.
33. Lu H and Van Zijl PCM. Experimental measurement of extravascular parenchymal BOLD effects and tissue oxygen extraction fractions using multi-echo VASO fMRI at 1.5 and 3.0 T. *Magn Reson Med* 2005; 53: 808–816.
34. Lajoie I, Tancredi FB and Hoge RD. Regional reproducibility of BOLD calibration parameter M, OEF and resting-state CMRO2 measurements with QUO2 MRI. *PLoS One* 2016; 11: 1–31.
35. Aizenstein HJ, Clark KA, Butters MA, et al. The BOLD hemodynamic response in healthy aging. *J Cogn Neurosci* 2004; 16: 786–793.
36. Esposito MD, Zarahn E, Aguirre GK, et al. The effect of normal aging on the coupling of neural activity to the bold hemodynamic response. *Neuroimage* 1999; 14: 6–14.
37. West KL, Zuppichini MD, Turner MP, et al. BOLD hemodynamic response function changes significantly with healthy aging. *Neuroimage* 2019; 188: 198–207.
38. Rypma B and D'Esposito M. Age-related changes in brain–behaviour relationships: evidence from event-related functional MRI studies. *Eur J Cogn Psychol* 2001; 13: 235–256.
39. Jenkinson M, Beckmann CF, Behrens TEJ, et al. Fsl. *Neuroimage* 2012; 62: 782–790.
40. Tabesh A, Jensen JH, Ardekani BA, et al. Estimation of tensors and tensor-derived measures in diffusional kurtosis imaging. *Magn Reson Med* 2011; 65: 823–836.
41. Smith SM, Johansen-Berg H, Jenkinson M, et al. Acquisition and voxelwise analysis of multi-subject diffusion data with tract-based spatial statistics. *Nat Protoc* 2007; 2: 499–503.
42. Mori S, Oishi K, Jiang H, et al. Stereotaxic white matter atlas based on diffusion tensor imaging in an ICBM template. *Neuroimage* 2008; 40: 570–582.
43. Yekutieli D and Benjamini Y. Resampling-based false discovery rate controlling multiple test procedures for correlated test statistics. *J Stat Plan Inference* 1999; 82: 171–196.
44. Leys C, Ley C, Klein O, et al. Do not use standard deviation around the mean, use absolute deviation around the median. *J Exp Soc Psychol* 2013; 49: 764–766.
45. Gauthier CJ, Madjar C, Tancredi FB, et al. Elimination of visually evoked BOLD responses during carbogen inhalation: implications for calibrated MRI. *Neuroimage* 2011; 54: 1001–1011.
46. Lin A-L, Fox PT, Yang Y, et al. Evaluation of MRI models in the measurement of $CMRO_2$ and its relationship with CBF. *Magn Reson Med* 2008; 60: 380–389.
47. Zou KH, Warfield SK, Bharatha A, et al. Statistical validation of image segmentation quality based on a spatial overlap index. *Acad Radiol* 2004; 11: 178–189.
48. De Stefano N. Axonal damage correlates with disability in patients with relapsing-remitting multiple sclerosis. Results of a longitudinal magnetic resonance spectroscopy study. *Brain* 1998; 121: 1469–1477.
49. Tomassini V, Johansen-Berg H, Jbabdi S, et al. Relating brain damage to brain plasticity in patients with multiple sclerosis. *Neurorehabil Neural Repair* 2012; 26: 581–593.
50. Toyokura M, Muro I, Komiya T, et al. Relation of bimanual coordination to activation in the sensorimotor cortex and supplementary motor area: analysis using functional magnetic resonance imaging. *Brain Res Bull* 1999; 48: 211–217.
51. Stefanovic B, Warnking JM and Pike GB. Hemodynamic and metabolic responses to neuronal inhibition. *Neuroimage* 2004; 22: 771–778.
52. Filippi M, Rocca MA, Colombo B, et al. Functional magnetic resonance imaging correlates of fatigue in multiple sclerosis. *Neuroimage* 2002; 15: 559–567.
53. Rocca MA, Meani A, Riccitelli GC, et al. Abnormal adaptation over time of motor network recruitment in multiple sclerosis patients with fatigue. *Mult Scler J* 2016; 1144–1153.